

RGB-D Salient Object Detection Based on Discriminative Cross-modal Transfer Learning

Hao Chen, Y.F. Li, and Dan Su
City University of Hong Kong

Abstract

In this work, we propose to utilize Convolutional Neural Networks (CNNs) to boost the performance of depth-induced salient object detection by capturing the high-level representative features for depth modality. We formulate the depth-induced saliency detection as a CNN-based cross-modal transfer problem to bridge the gap between the “data-hungry” nature of CNNs and the unavailability of sufficient labeled training data in depth modality. In the proposed approach, we leverage the auxiliary data from the source modality (i.e., RGB) effectively by training the RGB saliency detection network to obtain the task-specific pre-understanding layers for the target modality (i.e., depth). Meanwhile, we exploit the depth-specific information by pre-training a modality classification network that encourages modal-specific representations during the optimizing course. Thus, it could make the feature representations of the RGB and depth modalities as discriminative as possible. These two modules are pre-trained independently and then stitched to initialize and optimize the eventual depth-induced saliency detection model. Experiments demonstrate the effectiveness of the proposed novel pre-training strategy as well as the significant and consistent improvements of the proposed approach over other state-of-the-art methods.

1. Introduction

Salient object detection, aiming at modeling the attention mechanism of human visual systems to discriminate objects in the scene over their surroundings, has been applied in various areas such as image compression [1], object tracking [2] and object recognition [3] in recent years.

Biological research has proven that locations in the visual field that stand out over other regions are more likely to attract human attention [4-6]. Inspired by this principle, most traditional salient object detection models localize salient objects by evaluating the distinctiveness of a location with low-level visual features or searching for regions/objects that are distinctive from the background in

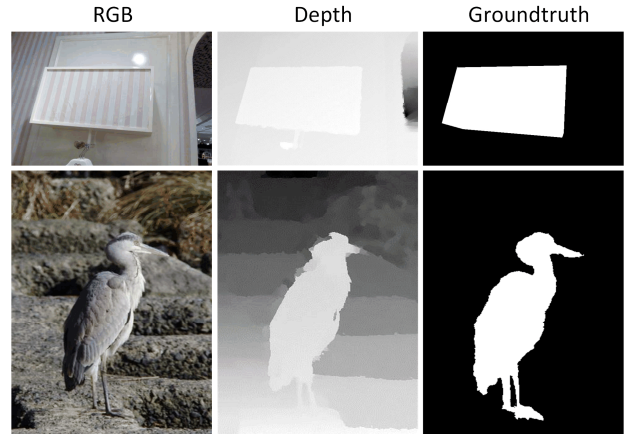


Figure 1: Examples to show the effectiveness of depth in salient object detection. The depth maps can provide clear edges though the appearances of salient object and background are similar.

RGB images [7-9]. These RGB-based saliency models may often fail when there is no clear contrast between foreground objects and the background as shown in two examples of Figure 1. However, for these examples, the depth information could provide useful cues for detecting saliency, which has not been well-explored by traditional salient object detection models.

Benefiting from the advantage of the off-the-shelf RGB-D sensors, the depth information has been successfully applied in saliency detection [10-17]. Typically, their saliency detection models directly leverage raw depth value or low-level hand-crafted features limited in understanding the global context in scenes. By contrast, the deep learning techniques especially Convolutional Neural Networks (CNNs) are acknowledged as quite competitive solutions with their powerful capacity in exploring high-level representations and complex correlations of multiple modalities.

Although CNNs are powerful in digging representative features and have been applied to various computer vision tasks [18-20] successfully, specific designs on CNNs for depth modality is still under-studied, especially for tackling the conflict between the ‘data-hungry’ nature of deep neural networks and the insufficiency of labeled data in depth

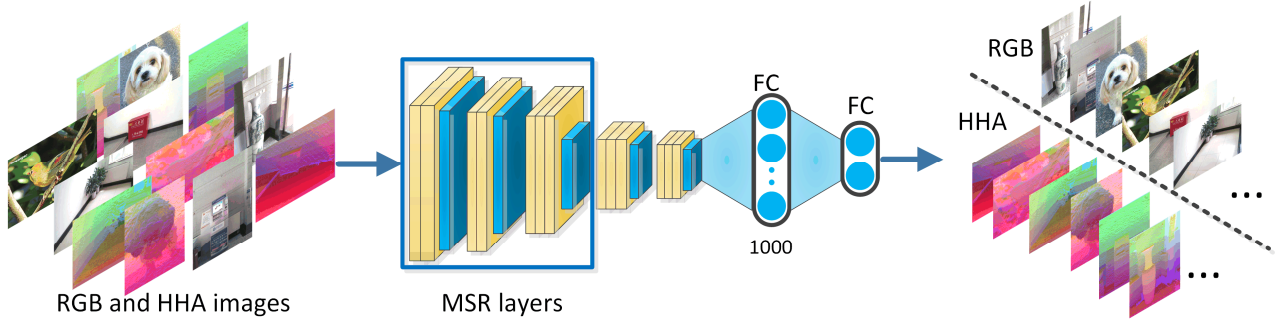


Figure 2: Flowchart of the modality classification network (MCNet). The low layers (from Conv1_1 to Conv3_3) of MCNet that highlighted in blue block will serve as modality-specific representation (MSR) layers in the stitched discriminative distillation network.

modality. Current paradigms for recognition in the computer vision community involve learning a generic feature representation on a large dataset with labeled images (e.g., ImageNet), and then specializing or fine-tuning the learned generic feature representation for the specific task [21]. Successful applications of this paradigm could be found in almost all state-of-the-art vision systems such as object detection and segmentation. As the most typical transfer learning strategy, fine-tuning an intact source model can guarantee a decent performance across tasks (e.g., from image classification to object detection) or across domains within the same modality (i.e., RGB).

Albeit that CNNs trained on RGB modality might be directly applied to depth-induced saliency detection due to the complementarity between RGB and depth modalities and the shared understanding in saliency detection task, it is reasonable to believe that the performance of CNN-based saliency detection will upgrade if the diversities between RGB and depth modalities in terms of data distribution, structure and appearance can be taken into account additionally. Therefore, an effective transfer strategy to explore and protect modal-specific representations for depth is on the demand.

To solve this problem, we propose a discriminative distillation transfer scheme to distill the task-specific understanding from the source data (i.e., RGB modality). Meanwhile, we explore the modal-specific representations for depth. We first formulate a modality classification network (MCNet) to capture the distinctiveness of the depth modality with only inexpensive modality labels (no paired relationship is required). The modality classification loss function is adopted to maximize the \mathcal{H} -divergence [22] across modalities, thus encouraging the emergence of discriminating modal-specific features in the optimization process.

Meanwhile, to empower task-specific (i.e., saliency detection) understanding of depth modality, we train a task knowledge transfer network (TKTNet) with RGB images to capture high-level understanding on saliency detection and

then truncate the high layers of the TKTNet as pre-understanding towards saliency detection for depth modality. Then the lower layers of MCNet is stitched with the high layers of the TKTNet, which is based on the observation that lower layers in CNNs are more modal-specific and task-agnostic while higher layers are more task-specific and modal-agnostic [21, 23]. By this way, the stitched network is expect to be initially endowed with the superior capacity for extracting discriminative features in depth modality and understanding of saliency detection task. We refer to the stitched network as discriminative distillation network (DDNet) and then fine-tune it with labeled depth images. When we fine-tune the DDNet, another supervision branch is added in the intermediate layers to facilitate learning modal-specific hidden structure and simultaneously improve the directness and transparency of the whole transfer learning process.

In this paper, we propose a novel computational model to detect salient objects from depth images, which utilizes CNNs to learn the high-level representation of depth modality. Compared with previous works, the proposed work has three major contributions:

(1) We introduce a novel discriminative distillation transfer scheme to inherit task-specific pre-understanding capacity, meanwhile capturing the depth-specific representations. The discriminative distillation transfer scheme that is implemented with only unpaired modality labels can serve as a promising solution for more cross-modal and cross-domain transfer learning problems.

(2) A hidden supervision transfer strategy for CNNs is proposed to guide the learning process of hidden structure. It could improve the directness and transparency of the whole transfer learning process simultaneously.

(3) As a pioneering deep learning-based depth-induced saliency detection exploration, our method, which only employs the depth information in the testing phase, outperforms other state-of-the-art salient object detection methods based on RGB-D images.

2. Related Works

2.1. Saliency detection in RGB images

Saliency detection methods can be coarsely categorized into bottom-up and top-down methods. Bottom-up methods make use of low-level visual cues like color, orientation and texture to measure the rarity of a pixel or region by local [4, 8], global [7, 9] or background prior [24, 25] contrast. Top-down methods [5, 6] are based on high-level task-specific prior knowledge. Recently, deep learning-based saliency detection methods [26-28] have achieved great improvements in each of the performance categories. Instead of manually defining and tuning saliency specific features, the deep learning-based methods can learn both low-level features and high-level semantics used for saliency detection straightly from minimally processed images. However, most of these works follow the traditional fine-tuning paradigm on RGB images and cross-modal problem is not involved in their investigations.

2.2. Saliency detection in RGB-D images

Most existing approaches for saliency detection based on RGB-D images either treat the depth map as an indicator to weight the RGB saliency map or consider depth cues as an independent image channel.

Ciptadi *et al.* [11] construct 3D layout and shape features as additional contrast cues and set fixed weights for the region contrast value. In [14], the depth weighted color contrast is employed to address the problem that the appearances between regions are similar. However, it is roughly assumed that the closer distance is associated with a larger saliency weight, which can hardly be generalized to all the images. Peng *et al.* [16] propose a multiple-layer optimal strategy for RGB-D saliency detection by simply serializing the RGB feature and depth value together as input, while ad-hoc consideration and designs for depth modality are unexplored. Ju *et al.* [13] measure the saliency of a point by calculating the contrast of depth values with its surroundings, which is not able to produce good results when a salient object shows low depth contrast with respect to the rest of the scene. Feng *et al.* [17] propose a depth saliency feature named Local Background Enclosure (LBE) to model the salient structure. This feature quantifies the proportion of the object boundary from the depth modality. However, this model cannot achieve a decent result when the salient object is embedded in the background with the short depth. It should be noted that notwithstanding the demonstrated success of these models, they do not go beyond the low-level contrast paradigm. Consequently, it still has much room for improvement via exploring high-level representations. Qu *et al.* [29] adopt Convolutional Neural Network technique to train a saliency

map integration model, in which hand-designed saliency features from RGB and depth modalities are fed into a CNN collectively to generate fused RGBD hyper-features. However, this model only focuses on the feature integration while specific exploration and designs for depth modality is beyond discussion.

2.3. Cross-modal Transfer learning

Within the same modality, domain adaptation techniques generally focus on improving the generalization of models or features learned on source domain by training a shared cross-domain dictionary [30], transforming target features to a new domain-invariant representation [31] or mapping target features into the source domain [32].

As for cross-modal transfer problems, Ngiam *et al.* [33] learn a shared representation between different modalities to capture relating information from them. Frome *et al.* [34] embed representations from multiple modalities into a shared feature space. Hoffman *et al.* [35] design a hallucination network branch to mimic depth mid-level features as the complementary information of RGB modality.

More recently, inspired by the network “distillation” technique proposed in [36], Gupta *et al.* [21] generalize this idea to cross-modal problems by utilizing the mid-level representations from the labeled modality as supervision to guide the learning of representations on the paired un-labeled modality. However, the pre-training procedure needs training images from different modalities to be paired, which is not required in our pre-training scheme.

All the works along this line mainly focus on using complementary knowledge or shared representation across modalities, which ignore exploiting and protecting specific representations of target modality. In contrast, our work here takes these two considerations into account jointly.

3. The Proposed approach

To tackle the challenge that labeled data of depth modality is insufficient for training a large CNN, we firstly train the MCNet (as shown in Figure 2) and TKTNet (as shown in Figure 3) to capture modality-specific representations and distill task-specific high-level understandings for depth modality, respectively. Then the low layers of the MCNet and the high layers of the TKTNet are connected together as the initialization to train a depth-induced salient object network (i.e., the DDNet shown in Figure 4). To further guarantee the comprehensive exploration of hidden structures and representations, we introduce another supervision in the hidden layer of the DDNet to enhance the learning of hidden structure and improve the optimizing directness and transparency.

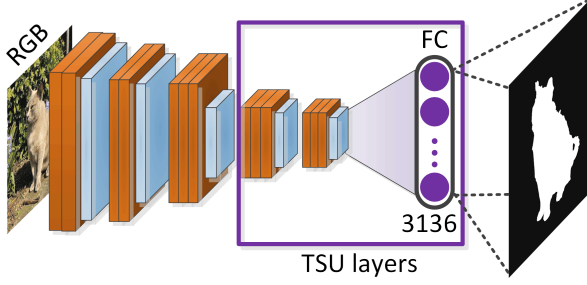


Figure 3: Flowchart of the task knowledge transfer network (TKTNet). The high layers (from Conv4_1 to FC) of the TKTNet that highlighted in purple block will serve as task-specific understanding (TSU) layers in the stitched discriminative distillation network (DDNet).

3.1. Modality classification network

To measure the disparity between RGB modality and depth modality, the \mathcal{H} -divergence applied in the same modality in [22, 37] is extended to our cross-modal transfer problems here. Given the distributions of RGB modality \mathcal{M}_R^x and depth modality \mathcal{M}_D^x over the input X and a hypothesis class \mathcal{H} of binary classifiers $\eta: X \rightarrow \{0,1\}$, the \mathcal{H} -divergence between \mathcal{M}_R^x and \mathcal{M}_D^x can be represented as

$$d_{\mathcal{H}}(\mathcal{M}_R^x, \mathcal{M}_D^x) = 2 \sup_{\eta \in \mathcal{H}} \left| \Pr_{X \sim \mathcal{M}_R^x} [\eta(x)=1] - \Pr_{X \sim \mathcal{M}_D^x} [\eta(x)=1] \right| \quad (1)$$

From Equation (1), it can be noted that the \mathcal{H} -divergence relies on the capacity of the hypothesis \mathcal{H} to distinguish between samples from \mathcal{M}_R^x and the ones from \mathcal{M}_D^x . As proved in [22], the empirical \mathcal{H} -divergence can be calculated by

$$\hat{d}_{\mathcal{H}}(\mathcal{M}_R^x, \mathcal{M}_D^x) = 2 \left(1 - \min \left[\frac{1}{n_1} \sum_{i=1}^{n_1} I[\eta(X_i)=0] + \frac{1}{n_2} \sum_{i=n_1+1}^N I[\eta(X_i)=1] \right] \right) \quad (2)$$

where $I[\eta(X_i)=0]$ is the binary indicator function which is 1 when $\eta(X_i)=0$ is true, and 0 otherwise. n_1 and n_2 denote the numbers of the samples in RGB and depth modalities respectively and $N=n_1+n_2$.

It is hard to optimize Equation (2) directly. However, the “min” part of Equation (2) suggests that, for maximum modality disparity to be achieved, predictions should be made based on features that can discriminate between two modalities. The pivot of our approach is to implement this idea in the context of neural network architectures by training on a collection of RGB and depth images with only modality labels. During the training phase, the MCNet promotes the emergence of features which can effectively discriminate depth images from RGB ones. Specifically, a binary classifier $\Theta(X_i|\Phi^M)$ that built on a modality classification network $\Phi^M=(\mathbf{W}^M, \mathbf{b}^M)$ with trainable weights

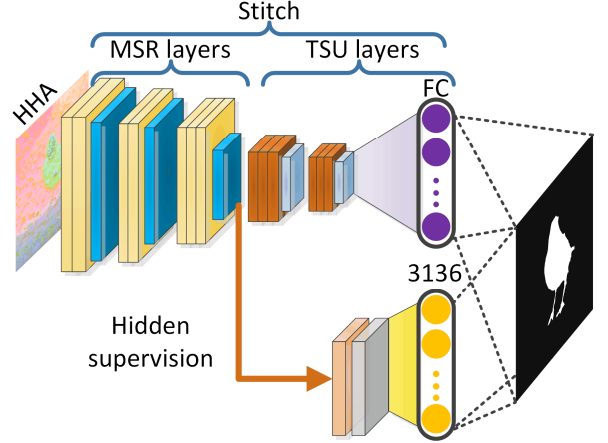


Figure 4: Flowchart of the discriminative distillation network (DDNet), which contains discriminative modality-specific representation (MSR) layers and task-specific understanding (TSU) layers that are truncated from MCNet and TKTNet respectively. The brown arrow introduces the hidden supervision branch.

\mathbf{W}^M and biases \mathbf{b}^M is trained by adopting *softmax* loss as the classification loss naturally:

$$\mathcal{L}(y, \Theta) = -\log \left(\frac{e^{\Theta_y}}{\sum_{j=1}^m e^{\Theta_j}} \right), \quad (3)$$

where m donates the modality numbers. By substituting $\Theta(X_i|\Phi^M)$ into Equation (2), the \mathcal{H} -divergence can be reformulated as

$$\hat{d}_{\mathcal{H}}(\mathcal{M}_R^x, \mathcal{M}_D^x) = 2 \left(1 - \min \left[\frac{1}{n_1} \sum_{i=1}^{n_1} I[\Theta(X_i | \Phi^M) = 0] + \frac{1}{n_2} \sum_{i=n_1+1}^N I[\Theta(X_i | \Phi^M) = 1] \right] \right) \quad (4)$$

Consequently, the min part of Equation (4) can be approximated by minimizing $\mathcal{L}(y, \Theta)$ on the training set, thus generating a maximum \mathcal{H} -divergence and encouraging discriminative representation for each modality.

To make full use of the depth modality, we first embed the original depth value to the three-channel HHA representation [38] (which encodes horizontal disparity, height above ground, and the angle of the local surface normal with the inferred gravity direction). Throughout this paper, we stick with using HHA embedding to represent the input depth images for its priority over the initial depth value that has been proven in [21]. We adopt VGG-16 [39] model as our basic architecture in our experiments. The initial VGG-16 model contains 13 convolution layers (denoted by orange in Figure 2), 5 max-pooling layers (denoted by blue) and 3 fully connected layers. We replace its fully connected layers with two new adaptation fully

connected (FC) layers for our task which contain 1000 and 2 nodes respectively.

Meanwhile, the training dataset for MCNet is constructed by picking up images from RGB and depth modalities randomly. The samples from RGB modality will be labeled as class 1, while samples from depth modality (HHA images) will be labeled as class 0.

3.2. Task knowledge transfer network

As shown in Figure 3, the architecture of task knowledge transfer network (TKTNet) is also based on VGG-16 architecture with modifications on fully connected (FC) layers to adapt saliency detection task. The adaptation FC layer consists of 3136 nodes and maps the high-level representations to saliency probabilities by sigmoid activation function. The 3136 saliency probabilities are then warped to a saliency map with size of 56×56 . To guarantee receptive field of each output node is the entire input image, the cross-entropy loss is then adopted, which incorporates the structural and global disparity between the whole predicted saliency map and the whole ground truth saliency mask. In this way, the saliency value of each pixel can be optimally estimated by considering the global context, thus avoiding the distraction of local salient patterns. The effectiveness of this global structural and its priority over fully convolutional layer in saliency detection task has been proven in [27].

3.3. Discriminative distillation network

After training the MCNet and TKTNet, we stitch the modality-specific representation (MSR) layers (Conv1_1 to Conv3_3) of the trained MCNet and the task-specific understanding (TSU) layers (from Conv4_1 to FC) of the trained TKTNet together (shown in Figure 4). Then we fine-tune it with only depth (HHA) images.

Inspired by the deeply-supervised net (DSN) [40], which aims at improving the transparency of optimization process for deep learning, we add a hidden supervision after the pooling 3 layer as a net surgery on the discriminative distillation network (DDNet). Specifically, we first add a new convolution layer with 128 3×3 convolutional kernels to reduce the size of the weights of the fully connected layer to save the memory and prevent overfitting. Besides, we append a dropout layer after the new convolution layer with the dropout rate set to 0.3. Thus the combined loss function containing the output loss and the hidden supervision loss can be described as:

$$L(\{\mathbf{I}_i^D, \mathbf{Y}_i\}_N | \Theta^D) = \lambda_1 \cdot L(\{\mathbf{I}_i^D, \mathbf{Y}_i\}_N | \Theta^{D,1}) + \lambda_2 \cdot L(\{\mathbf{I}_i^D, \mathbf{Y}_i\}_N | \Theta^{D,2}), \quad (5)$$

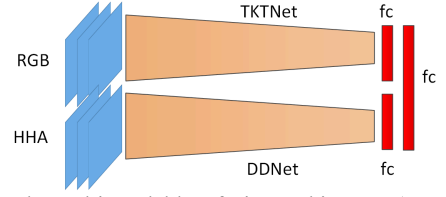


Figure 5: The multi-modal late fusion architecture ('MMNet').

where $\{\mathbf{I}_i^D\}_N$ indicates the input training HHA images of depth modality, $\Theta^{D,1}$ and $\Theta^{D,2}$ represent the parameters of each part, respectively. The hidden supervision loss also employs the cross entropy loss and the two parts of losses can be presented with the same form and are weighted by λ_1 and λ_2 , respectively. We directly set $\lambda_1 = \lambda_2 = 1$ without further tuning. It should be noted that the same ground truth is being used for the hidden supervision loss and output loss.

3.4. Multi-modal fusion network

To fairly compare with other RGBD saliency detection models, we add the RGB modality through a late fusion mode (shown in Figure 5), which means connecting the TKTNet (RGB stream) and DDNet (depth stream) after their fully connected layer (denoted as 'fc') by adding a new fully connected layer (denoted as 'fc') with 3136 nodes to learn multi-modal fusion results (indicated as 'MMNet').

4. Experiments

4.1. Datasets

We evaluate the effectiveness of our model on four public benchmark datasets:

DES [41] contains 135 RGB-D image pairs and corresponding groundtruth. All the image pairs in this dataset are used to test.

NLPR [16] consists of 1000 image pairs, each of which contains single or multiple salient objects, including indoor and outdoor scenes under different illumination conditions. We randomly choose 650 image pairs from this dataset for training, 50 image pairs for validation and 300 image pairs for testing.

NJUD [13] contains 2003 image pairs collected from Internet, 3D movies and photographs. We randomly select 1400 images from the this dataset as the training samples, 100 image pairs for validation and 503 image pairs for testing.

STEREO [42] provides the web links for downloading stereoscopic images and also provides the manually segmented ground truth. We download a total of 797 pairs of binocular images from all the available web links to construct a dataset. We also use all the image pairs in this dataset for testing.

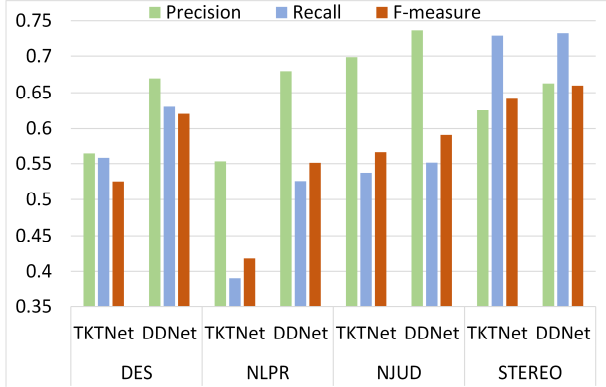


Figure 6: Quantitative comparisons of the TKTNet and DDNet on four public datasets without fine-tuning.

Stitching point	DES	NLPR	NJUD	STEREO
Conv1_2	0.527	0.472	0.586	0.657
Conv2_2	0.605	0.520	0.585	0.663
Conv3_3	0.621	0.551	0.591	0.642
Conv4_3	0.578	0.563	0.558	0.535
Conv5_3	0.488	0.466	0.509	0.498

Table 1: F-measure scores of the DDNet in terms of choosing different stitching points.

Notably, the depth images in both NLPR and DES datasets are generated by Kinect, while depth images in NJUD and STEREO datasets are disparity maps that computed from the stereo image pairs. Considering the difference between disparity maps and depth maps in terms of data distribution, we separately train two series of models with two types of datasets respectively.

4.2. Evaluation metrics

To evaluate the effectiveness of the proposed method, we adopt Precision-Recall (PR) curve and F-measure as evaluation metrics. To further evaluate the performance of the proposed method for salient object segmentation, we report the performance of segmenting the saliency map using a self-adaptive threshold. We set the threshold $T = \mu + \varepsilon$ as suggested in [43], where μ and ε are the mean value and the standard deviation of the saliency map, respectively. The formulation of F-measure is

$$F_{\beta} = \frac{(1 + \beta^2) \cdot \text{Precision} \cdot \text{Recall}}{\beta^2 \cdot \text{Precision} + \text{Recall}}, \quad (6)$$

where we set $\beta^2=1$ as suggested in [44].

4.3. Implementation details

When we train the MCNet, all the training samples are used. It is also necessary to augment the dataset since the amount of all existing RGB-D salient object detection

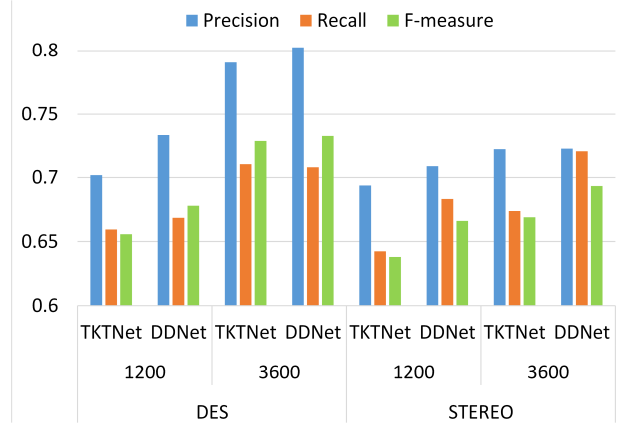


Figure 7: Quantitative comparisons of the fine-tuned models initialized by TKTNet and DDNet respectively. We change the number of training samples from 1200 to 3600.

	DES	NLPR	NJUD	STEREO
w/o HS	0.724	0.736	0.737	0.691
w HS	0.769	0.746	0.744	0.723

Table 2: F-measure scores of the DDNet with adding hidden supervision or not.

datasets is seriously insufficient. We implement the image augmentation by 12 times via horizontally-flipping and image cropping on the training samples.

We set the size of mini-batch to 4 for the limited GPU memory. Besides, we set weight decay, and momentum to, 0.0002, and 0.9, and the training rate for MCNet, TKTNet and DDNet is 0.001, 0.0000005 and 0.00000005 respectively. We implement our models with caffe [45] toolbox on a workstation with a GTX TITAN X GPU.

4.4. Evaluation of the proposed transfer strategies

The effectiveness of discriminative distillation transfer scheme. To confirm the effectiveness of the discriminative distillation transfer scheme, we compare two models with HHA images as inputs: the initial stitched DDNet without further fine-tuning and the TKTNet trained on RGB modality. The difference between these two models only lies in the low layers (Conv1_1 to Conv3_3). The experimental results shown in Figure 6 demonstrate that the DDNet without fine-tuning outperforms TKTNet by a large margin (more than 0.1 in terms of F-measure for some datasets), which is consistent with our assumption that the initial DDNet that incorporates the MSR layers pre-trained by MCNet is more likely to provide discriminative depth-specific representations than the TKTNet that are only trained with RGB images. This boosting also demonstrates that our discriminative distillation transfer scheme has strong potentiality to be applied to the zero-shot learning problems.

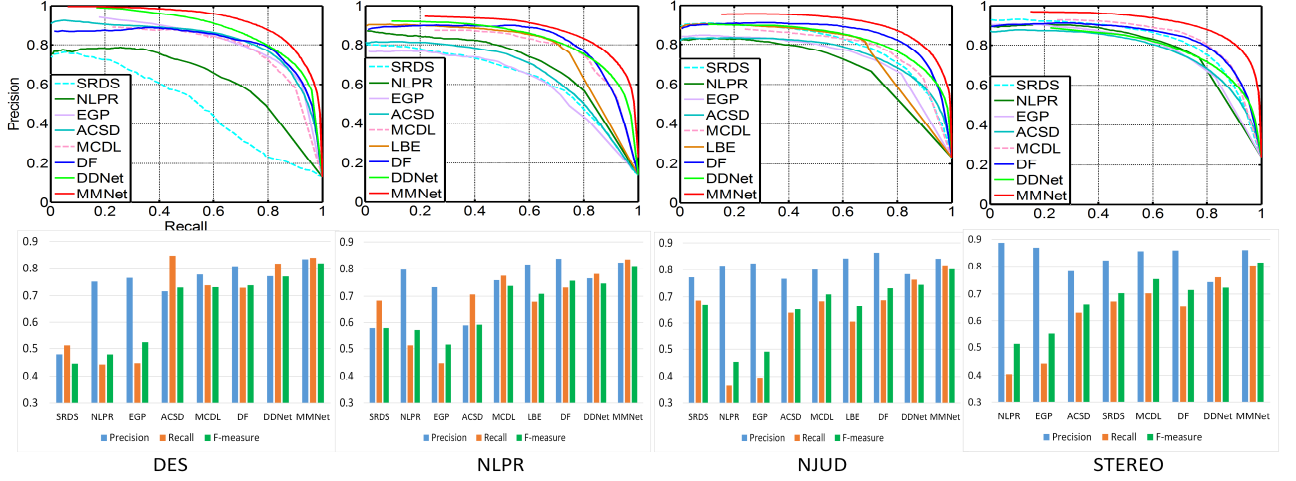


Figure 8: PR curves and F-measure scores that are compared to other saliency detection models.

To further validate the effectiveness of the proposed discriminative distillation transfer scheme, we fine-tune the TKTNet and DDNet using HHA images, respectively. We compare the performance of our proposed transfer method on DES and STEREO datasets, which do not contribute any training samples and consequently can gauge the generalization capacity of trained models. Moreover, we adjust the scale of training data to observe the changes in the prediction performance of DDNet and TKTNet with respect to the number of training data. As shown in Figure 7, the fine-tuned DDNet typically works better than the fine-tuned TKTNet due to the more discriminative depth-specific representations in low layers explored by the pre-trained MCNet. Figure 7 also indicates that with the decreasing number of training samples, our discriminative distillation transfer scheme shows greater advantages over fine-tuning TKTNet.

The choice of stitching point. Another question in our discriminative distillation transfer scheme is that how performance varies as the stitching point is changed. To answer this question, we vary the connecting point and test the corresponding performances. As shown in Table 1, it can generally achieve a satisfactory performance by choosing Conv3_3 as the connecting point. Such a choice resonates well with the observation in [23] that lower layers in CNNs are more modality-specific and task-agnostic (and thus more suitable to be transferred from across tasks rather than across modalities), while the higher layers possess the opposite properties. It also validates our motivation that there should be a good balance between task-specific understanding and modality-specific representation when initializing a cross-modal task.

The effectiveness of the hidden supervision strategy. As shown in Table 2, the F-measure scores with or without hidden supervision (HS) on four datasets validate its

effectiveness in improving transfer learning performance.

According to our analysis, the reasons are as follows:

- (i) The HS strategy can further enhance the learning of hidden structure and simultaneously improve the directness and transparency of the whole transfer learning process.
- (ii) The HS strategy serves not only as a transfer learning strategy, but also can be seen as an additional (soft) constraint within the learning process. This constraint can act as a new regularization to prevent possible overfitting, especially on the condition of small training data.

4.5. Comparison to other saliency models

We compare the proposed DDNet with 5 state-of-the-art RGB-D salient object detection models, including DF [29], LBE¹ [17], NLPR [16], SRDS [14] and EGP [15], one depth-induced salient object detection model ACSD [13], as well as one state-of-the-art CNN-based RGB saliency detection model MCDL [28]. The PR curves and F-measure scores shown in Figure 8 indicate that despite we utilize depth images only when testing without further refinements, our DDNet outperforms all other state-of-the-art models in general, including most RGB-D saliency detection models. Specifically, we compare the average F-measure scores on four public datasets with the most state-of-the-art RGB saliency, depth-induced saliency and RGB-D saliency detection models, respectively. The MCDL model, which leverages CNNs for RGB saliency detection, is among the best RGB salient object detection approaches. Although RGB image might contain more information than the depth, our DDNet model still outperforms MCDL with nearly 2% margin across the four datasets. Besides, the DF method utilizes CNNs for RGB-D saliency detection and integrates a Laplacian propagation framework for refinement, while

¹ LBE only provides the results on NLPR and NJUD datasets.

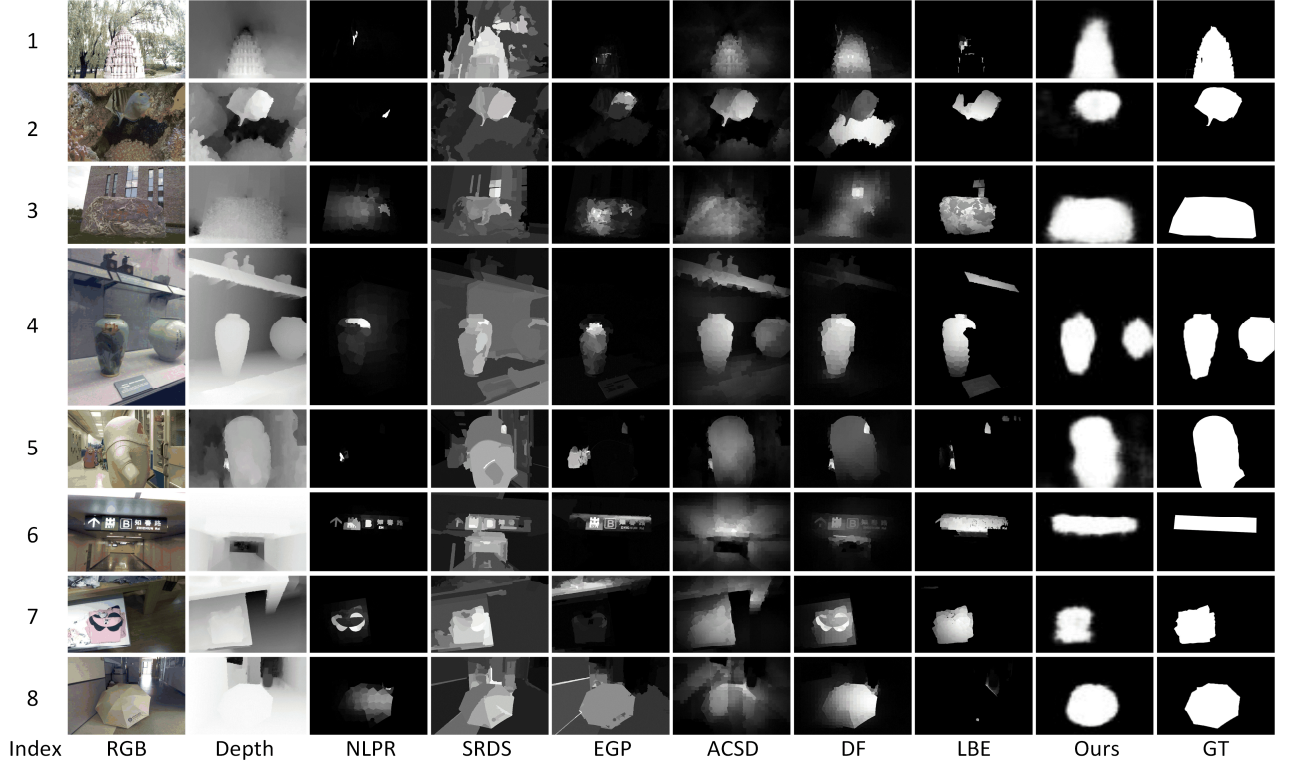


Figure 9: Visual comparisons of our model and other depth-induced and RGB-D saliency detection models.

our DDNet, which only uses depth image for testing and do not adopt any refinements, still outperforms the DF model (0.746 vs. 0.735) on most datasets. For the STEREO dataset, DF and MCDL show the better PR curves than our DDNet. It is probably due to that a considerable amount of salient regions are heavily determined by RGB information in this dataset since the MCDL method with the RGB modality performs better than the DF model with RGB-D modality only on this dataset. We attribute the superiority of our DDNet to the well-transferred task-specific pre-understanding and well-explored features for depth modality. Our MMNet incorporating RGB and depth modalities further outperforms others with a significant margin.

As shown in Figure 9, on various conditions of the complex background (the 1th-2th row), the similar appearance between backgrounds and the salient object (the 3th row), multiple objects (the 4th row), large salient regions touching the boundaries (the 5th row), small depth value discrimination with background (the 6th-7th row) and large depth value range in salient objects (the 8th row), our model can still localize the salient object accurately and generate a coherent and precise saliency map effectively by exploiting powerful representations in depth modality for saliency detection. By contrast, other models tend to fail on these challenging conditions for their ungeneralizable hand-crafted features in depth modality or heuristic and

simple modelling for the relationship between depth and saliency. These hand-crafted features lack high-level global understanding (e.g., objectness) for complex scenes and are prone to be affected by distractions from local-salient patterns and non-uniform distribution of salient objects.

5. Conclusions

In this work, we propose to utilize CNNs to capture the high-level representative features for depth modality and formulate the depth-induced saliency detection as a cross-modal transfer problem. A novel discriminative distillation transfer scheme is introduced to capture task-specific pre-understanding and exploit depth-specific representations simultaneously. Experiments demonstrate the effectiveness of the proposed novel pre-training strategy and the significant and consistent improvements of the proposed approach over other state-of-the-art RGB-D saliency detection methods.

In addition, the approach proposed in this paper would enable us to effectively leverage new modalities given by other standard vision tasks, such as infra-red images from thermal sensors, aerial images from satellites and drones and LIDAR point clouds from laser scanners.

References

- [1] C. Guo and L. Zhang. A novel multiresolution spatiotemporal saliency detection model and its applications in image and video compression. *TIP*, vol. 19, pp. 185-198, 2010.
- [2] A. Borji, S. Frintrop, D. N. Sihite, and L. Itti. Adaptive object tracking by learning background context. in *CVPRW*, 2012.
- [3] Z. Ren, S. Gao, L.-T. Chia, and I. W.-H. Tsang. Region-based saliency detection and its application in object recognition. *IEEE Trans. CSVT*, vol. 24, pp. 769-779, 2014.
- [4] L. Itti, C. Koch, and E. Niebur. A model of saliency-based visual attention for rapid scene analysis. *PAMI*, pp. 1254-1259, 1998.
- [5] J. Yang and M.-H. Yang. Top-down visual saliency via joint CRF and dictionary learning. in *CVPR*, 2012.
- [6] L. Zhang, M. H. Tong, T. K. Marks, H. Shan, and G. W. Cottrell. SUN: A Bayesian framework for saliency using natural statistics. *Journal of vision*, vol. 8, pp. 32-32, 2008.
- [7] M. Cheng, N. J. Mitra, X. Huang, P. H. Torr, and S. Hu. Global contrast based salient region detection. *PAMI*, vol. 37, pp. 569-582, 2015.
- [8] J. Harel, C. Koch, and P. Perona. Graph-based visual saliency. in *NIPS*, 2006.
- [9] P. Jiang, H. Ling, J. Yu, and J. Peng. Salient region detection by ufo: Uniqueness, focusness and objectness. in *ICCV*, 2013.
- [10] Y. Cheng, H. Fu, X. Wei, J. Xiao, and X. Cao. Depth enhanced saliency detection method. in *ICIMCS*, 2014.
- [11] A. Ciptadi, T. Hermans, and J. M. Rehg. An in depth view of saliency. in *BMVC*, 2013.
- [12] K. Desingh, M. K. K., D. Rajan, and C. Jawahar. Depth really Matters: Improving Visual Salient Region Detection with Depth. in *BMVC*, 2013.
- [13] R. Ju, L. Ge, W. Geng, T. Ren, and G. Wu. Depth saliency based on anisotropic center-surround difference. in *ICIP*, 2014.
- [14] X. Fan, Z. Liu, and G. Sun. Salient region detection for stereoscopic images. in *DSP*, 2014.
- [15] J. Ren, X. Gong, L. Yu, W. Zhou, and M. Y. Yang. Exploiting global priors for RGB-D saliency detection. in *CVPRW*, 2015.
- [16] H. Peng, B. Li, W. Xiong, W. Hu, and R. Ji. Rgb-d salient object detection: a benchmark and algorithms. in *ECCV*, 2014.
- [17] D. Feng, N. Barnes, S. You, and C. McCarthy. Local background enclosure for RGB-D salient object detection. in *CVPR*, 2016.
- [18] D. Eigen, C. Puhrsch, and R. Fergus. Depth map prediction from a single image using a multi-scale deep network. in *NIPS*, 2014.
- [19] J. Long, E. Shelhamer, and T. Darrell. Fully convolutional networks for semantic segmentation. in *CVPR*, 2015.
- [20] S. Xie and Z. Tu. Holistically-nested edge detection. in *ICCV*, 2015.
- [21] S. Gupta, J. Hoffman, and J. Malik. Cross modal distillation for supervision transfer. *arXiv preprint arXiv:1507.00448*, 2015.
- [22] S. Ben-David, J. Blitzer, K. Crammer, A. Kulesza, F. Pereira, and J. W. Vaughan. A theory of learning from different domains. *Machine learning*, vol. 79, pp. 151-175, 2010.
- [23] K. Lenc and A. Vedaldi. Understanding image representations by measuring their equivariance and equivalence. in *CVPR*, 2015.
- [24] C. Yang, L. Zhang, H. Lu, X. Ruan, and M.-H. Yang. Saliency detection via graph-based manifold ranking. in *CVPR*, 2013.
- [25] J. Han, D. Zhang, X. Hu, L. Guo, J. Ren, and F. Wu. Background prior-based salient object detection via deep reconstruction residual. *IEEE Trans. CSVT*, vol. 25, pp. 1309-1321, 2015.
- [26] G. Lee, Y.-W. Tai, and J. Kim. Deep Saliency with Encoded Low level Distance Map and High Level Features. *arXiv preprint arXiv:1604.05495*, 2016.
- [27] N. Liu and J. Han. DHSNet: Deep Hierarchical Saliency Network for Salient Object Detection. in *CVPR*, 2016.
- [28] R. Zhao, W. Ouyang, H. Li, and X. Wang. Saliency detection by multi-context deep learning. in *CVPR*, 2015.
- [29] L. Qu, S. He, J. Zhang, J. Tian, Y. Tang, and Q. Yang. RGBD Salient Object Detection via Deep Fusion. *arXiv preprint arXiv:1607.03333*, 2016.
- [30] Y. Huang, F. Zhu, L. Shao, and A. F. Frangi. Color object recognition via cross-domain learning on RGB-D images. in *ICRA*, 2016.
- [31] J. Hoffman, E. Rodner, J. Donahue, T. Darrell, and K. Saenko. Efficient learning of domain-invariant image representations. *arXiv preprint arXiv:1301.3224*, 2013.
- [32] B. Kulis, K. Saenko, and T. Darrell. What you saw is not what you get: Domain adaptation using asymmetric kernel transforms. in *CVPR*, 2011.
- [33] J. Ngiam, A. Khosla, M. Kim, J. Nam, H. Lee, and A. Y. Ng. Multimodal deep learning. in *ICML*, 2011.
- [34] A. Frome, G. S. Corrado, J. Shlens, S. Bengio, J. Dean, and T. Mikolov. Devise: A deep visual-semantic embedding model. in *NIPS*, 2013.
- [35] J. Hoffman, S. Gupta, and T. Darrell. Learning with Side Information through Modality Hallucination. *arXiv preprint arXiv:1605.05395*.
- [36] G. Hinton, O. Vinyals, and J. Dean. Distilling the knowledge in a neural network. *arXiv preprint arXiv:1503.02531*, 2015.
- [37] Y. Ganin, E. Ustinova, H. Ajakan, P. Germain, H. Larochelle, F. Laviolette, M. Marchand, and V. Lempitsky. Domain-adversarial training of neural networks. *JMLR*, vol. 17, pp. 1-35, 2016.
- [38] S. Gupta, R. Girshick, P. Arbeláez, and J. Malik. Learning rich features from RGB-D images for object detection and segmentation. in *ECCV*, 2014.
- [39] K. Simonyan and A. Zisserman. Very deep convolutional networks for large-scale image recognition. *arXiv preprint arXiv:1409.1556*, 2014.
- [40] C.-Y. Lee, S. Xie, P. Gallagher, Z. Zhang, and Z. Tu. Deeply-Supervised Nets. in *AISTATS*, 2015.
- [41] Y. Cheng, H. Fu, X. Wei, J. Xiao, and X. Cao. Depth Enhanced Saliency Detection Method. in *ACM ICIMCS*, 2014.
- [42] Y. Niu, Y. Geng, X. Li, and F. Liu. Leveraging stereopsis for saliency analysis. in *CVPR*, 2012.

- [43] J. Guo, Z. Li, L.-F. Cheong, and S. Z. Zhou. Video co-segmentation for meaningful action extraction. in *ICCV*, 2013.
- [44] D. R. Martin, C. C. Fowlkes, and J. Malik. Learning to detect natural image boundaries using local brightness, color, and texture cues. *PAMI*, vol. 26, pp. 530-549, 2004.
- [45] Y. Jia, E. Shelhamer, J. Donahue, S. Karayev, J. Long, R. Girshick, S. Guadarrama, and T. Darrell. Caffe: Convolutional architecture for fast feature embedding. in *ACM MM*, 2014.